arXiv:1105.0300v1 [nucl-th] 2 May 2011

Dependence of elliptic flow on transverse momentum in $\sqrt{s_{NN}} = 200$ GeV Au-Au and $\sqrt{s_{NN}} = 2.76$ TeV Pb-Pb collisions

Bao-Chun Li*, Yuan-Yuan Fu, Er-Qin Wang, Fu-Hu Liu†

Department of Physics and Institute of Theoretical Physics,

Shanxi University, Taiyuan, Shanxi 030006, China

We investigate the dependence of elliptic flows v_2 on transverse momentum P_T for charged hadrons produced in nucleus-nucleus collisions at high energy by using a multi-source ideal gas model which includes the interaction contribution of the emission sources. Our calculated results are approximately in agreement with the experimental data over a wider P_T range from the STARand ALICE Collaborations. It is found that the expansion factor increases linearly with the impact parameter from most central (0-5%) to mid-peripheral (35-40%) collisions.

PACS numbers: 25.75.-q, 24.10.Pa, 25.75.Ld

Keywords: Azimuthal anisotropy, elliptic flow, multi-source ideal gas model

I. INTRODUCTION

The first elliptic flow data from the Large Hadron Collider(LHC) obtained by the ALICE Collaboration [1] are similar as observed at lower energies at the Relativistic Heavy Ion Collider (RHIC) [2, 3]. The elliptic flow of charged hadrons as a function of transverse momentum $v_2(P_T)$ increases with P_T and saturates at higher P_T. The similarity between the elliptic flows at LHC and RHIC is consistent with the predictions of the viscous hydrodynamic model [4]. The elliptic flow is generated in a collective expansion of the dense matter created in the collisions. The comparison to model calculations can provide valuable information of the collisional evolution. Recent results of relativistic viscous hydrodynamic calculations for Pb-Pb collisions at $\sqrt{s_{NN}} = 2.76$ shows systematic deviations from the ALICE data in the small momenta region $P_T < 800$ MeV [5]. The deviations is interpreted to be a non-negligible contribution of non-thermalized particles from jet fragmentation. The origin of this deviation is still under debate. Elliptic flow results from the interactions among the produced particles and can be used to probe local thermodynamic equilibrium. By fitting the experimental data of elliptic flows, it has been found in Ref. [6] that the average Quark Gluon Plasma (QGP) specific shear viscosity η/s slightly increases from RHIC to LHC energies in the newly developed hybrid model VISHNU, which connects viscous hydrodynamics with a hadron cascade model. At the LHC energies, it remains an open question whether the QGP fluid is more viscous or more perfect.

Elliptic flow is a measure of the azimuthal anisotropy of particle momentum distributions in the plane perpendicular to the beam direction. It results from the initial spatial anisotropy in non-central collisions and is thus sensitive to the properties of the hot dense matter formed during the initial stage of heavy ion collisions. In a thermodynamical picture, the asymmetric distribution of the initial energy density causes a larger pressure gradient in the shortest direction of the ellipsoidal medium, which can lead to an anisotropic azimuthal emission of particles. As a signature of collective flow in relativistic nuclear collisions, the elliptic flow was experimentally observed at the AGS, SPS, RHIC, and LHC,respectively [7–11]. In recent years, it has been believed that the system created at the RHIC [11] is a strongly coupled quark-gluon plasma (sQGP) and

* libc2010@163.com, s6109@sxu.edu.cn

† fuhuliu@163.com, liufh@mail.sxu.cn

behaves like a nearly "perfect" fluid by using the hydrodynamic simulation to the elliptic flow at the RHIC [12, 13].

II. MULTI-SOURCE IDEAL GAS MODEL

The multi-source ideal gas model is developed by us [14–16] from the Maxwell's ideal gas model. In this section, we briefly outline the calculation in the model. Many primary nucleon-nucleon collisions happen at the initial stage of nucleus-nucleus collisions. Each primary nucleon-nucleon collision can be regarded as an emission source (a compound hadron fireball) at intermediate energy or a few sources (wounded partons and woundless partons) at high energy. The participant nucleons that take part in primary collisions have probabilities to take part in cascade collisions with latter nucleons. Meanwhile, the particles produced in primary or cascade nucleon-nucleon collisions have probabilities to take part in secondary collisions with latter nucleons and other particles. Each cascade (or secondary) collision is also regarded as an emission source or a few sources. Many emission sources of final-state particles are expected to be formed in the collision process, and each source is considered to be a Maxwells ideal gas in the rest source frame. There are interactions among the emission sources due to the mechanics and electromagnetism effects. The interactions will cause the source to depart from the isotropic emission. To describe the anisotropic source, the sources deformation and movement in the model have been introduced.

Let the beam direction be the *oz* axis and the reaction plane be the *xoz* plane, which is spanned by the vector of the impact parameter and the beam direction. In the rest source frame, the three momentum components P'_x, P'_y, and P'_z of the considered particle have Gaussian distributions with the same standard deviation σ. The azimuthal anisotropy of particles produced in nuclear collisions can be described by the two momentum, P_x and P_y components in the transverse plane. The P_x and P_y distributions are given by

$$f_{P'_{x,y}}(P'_{x,y}) = \frac{1}{\sqrt{2\pi}\sigma} \exp\left[-\frac{P'^2_{x,y}}{2\sigma^2}\right]. \tag{1}$$

According to Gaussian momentum distribution, the width of the distribution $\sigma = \sqrt{TM}$, where T and M are the source temperature and particle mass respectively.

Due to the interactions with other emission sources, the considered source will have deformations and movements along the *ox* and *oy* axes, we have

$$P_x = A_x P'_x + B_x, \tag{2a}$$

$$P_y = A_y P'_y + B_y, \tag{2b}$$

where $A_{x,y}$ and $B_{x,y}$ represent the coefficients of source deformations along the *ox*(or *oy*) axis and movements along the corresponding axis respectively. The shifted deformable source is simply parameterized to have the linear relation between $P_{x,y}$ and $P'_{x,y}$, which reflects the mean result of source interaction. For a Maxwells ideal gas, $A_{x,y} = 1$ and $B_{x,y} = 0$, the source has no expansion and no contribution to the collective flow. For $A_{x,y} > 1$, the source expands, leading to an azimuthal anisotropy of the particle momentum distribution in the transverse plane. The amplitude of the azimuthal anisotropy can be measured by the elliptic flow, which is a sensitive probe of the final state interactions. For $B_{x,y}$, a positive value means source movements along the direction of the *ox* or *oy* axis, and a negative value indicates source movements along the opposite direction of the corresponding axis.

Generally speaking, different $A_{x,y}$ or $B_{x,y}$ can be obtained for events with different centralities or impact parameters. When two ultrarelativistic nuclei collide at non-zero impact parameter, their overlap area in the transverse plane has a short axis(*ox*), which is parallel to the impact parameter, and a long axis which is perpendicular to the

impact parameter. Elliptic flow in the central region of collisions is driven by the almond shape of the overlapping region [17–19]. This almond shape of the initial profile is converted by the pressure gradient into a momentum asymmetry. More particles are emitted along the short axis and the magnitude of this effect is characterized by A_x. The momentum anisotropy is largest in the early evolution of the collision. As the system expanding, the system becomes more spherical, and the driving force quenches itself gradually. With the increasing of P_x or P_y of the particles produced in the collisions, the momentum anisotropy decreases. So, for the concerned centrality, A_x is not a constant, but a function of the momentum. We set empirically the function

$$A_x(P_x, P_y) = 1 + k \exp\left(-\sqrt{(u_1 P_x)^2 + (u_2 P_y)^2}\Big/\sigma\right) \tag{3}$$

where the expansion factor k indicates the magnitude of the expansion, u_1 and u_2 denote the contributions of P_x and P_y respectively. When $k > 0$, we have $A_x > 1$, which renders the expansion of sources along the axis. When P_x(or P_y) increases to sufficiently large values, A_x closes to 1, which renders the momentum anisotropy vanishes and the elliptic flow $v_2 = 0$. The other parameters taken for calculations are $A_y = 1$ and $B_x = B_y = 0$, which is the default value.

The probability density function of $P_{x,y}$ is obtained as

$$f_{P_{x,y}}(P_{x,y}) = \frac{1}{\sqrt{2\pi}\sigma A_{x,y}} \exp\left[-\frac{(P_{x,y} - B_{x,y})^2}{2\sigma^2 A_{x,y}^2}\right]. \tag{4}$$

The corresponding transverse momentum and azimuth read as

$$P_T = \sqrt{P_x^2 + P_y^2} \tag{5}$$

and

$$\phi = \arctan\frac{P_y}{P_x} \tag{6}$$

respectively. With Eqs. (**??**), the joint probability density function of P_T and ϕ is given by

$$\begin{aligned} f_{P_T,\phi}(P_T, \phi) &= P_T f_{P_T,\phi}(P_T \cos\phi, P_T \sin\phi) \\ &= \frac{P_T}{2\pi\sigma^2 A_x A_y} \exp\left[-\frac{(P_T\cos\phi - B_x)^2}{2\sigma^2 A_x^2} - \frac{(P_T \sin\phi - B_y)^2}{2\sigma^2 A_y^2}\right] \end{aligned} \tag{7}$$

Considering the measurement in experiments, the elliptic flow in the model is defined as

$$v_2(P_T) = \langle\cos(2\phi)\rangle = \frac{\int_0^{2\pi} d\phi \int_{P_T - \frac{1}{2}\Delta P_T}^{P_T + \frac{1}{2}\Delta P_T} \cos(2\phi) f_{P_T,\phi}(P_T, \phi) dP_T}{\int_0^{2\pi} d\phi \int_{P_T - \frac{1}{2}\Delta P_T}^{P_T + \frac{1}{2}\Delta P_T} f_{P_T,\phi}(P_T, \phi) dP_T} \quad , \tag{8}$$

where ΔP_T is a given P_T bin. In the Monte Carlo calculation, we have

$$P'_{x,y} = \sigma\sqrt{-2\ln r_{1,3}}\cos(2\pi r_{2,4}) \tag{9}$$

where r_1, r_2, r_3, and r_4 denote random numbers in [0,1]. Using Eq. (2), (5), and (9), the transverse momentum and azimuthal angle can be represented as

$$P_T = \sqrt{\left[A_x\sigma\sqrt{-2\ln r_1}\cos(2\pi r_2) + B_x\right]^2 + \left[A_y\sigma\sqrt{-2\ln r_3}\cos(2\pi r_4) + B_y\right]^2} \tag{10}$$

and

$$\phi = \arctan\frac{A_y\sigma\sqrt{-2\ln r_3}\cos(2\pi r_4) + B_y}{A_x\sigma\sqrt{-2\ln r_1}\cos(2\pi r_2) + B_x} \quad , \tag{11}$$

respectively. The elliptic flow reads

$$v_2 = \langle \cos(2\phi) \rangle = \left\langle \frac{P_x^2 - P_y^2}{P_x^2 + P_y^2} \right\rangle. \tag{12}$$

III. COMPARISONS WITH EXPERIMENTAL DATA

The dependences of elliptic flows v_2 on transverse momentum P_T for charged particles produced in Au-Au collisions at $\sqrt{s_{NN}} = 200$ GeV are presented in Fig.1 The symbols are the experimental data of the STAR Collaboration [2] in eleven collision centralities. Our results are shown as the curves. The parameters used for calculations and the corresponding χ^2 per degree of freedom (χ^2/dof) are given in Table I. In the calculation, the values of σ and k are determined by fitting the model to the data, the values of u_1 and u_2 are taken to be 0.944 and 0.59-0.61 respectively, which is independent on centrality. It is obvious that v_2 increases with P_T in the low P_T region, as predicted by ideal hydrodynamic calculations. The observed v_2 saturates or decreases in the region of $P_T > 2$ GeV/c. However, ideal hydrodynamic model calculations show that v_2 increases with P_T in this region [20]. One can see that the calculated results are approximately in agreement with the experimental data on the dependence of v_2 on P_T in the whole observed P_T region for all concerned centralities. The expansion factor k increases and the momentum distribution width σ decreases with the centrality percent. According to $\sigma = \sqrt{TM}$, we can say that the source temperature T increases with the centrality.

In Fig. 2, we show elliptic flows v_2 as a function of the transverse momentum P_T for charged hadrons produced in Pb-Pb collisions at $\sqrt{s_{NN}} = 2.76$ TeV [1]. The symbols are the experimental results obtained with 4-particle cumulant methods and denoted as $v_2\{4\}$. The elliptic flow of charged hadrons measured by the ALICE Collaboration as a function of transverse momentum $v_2(P_T)$ is nearly identical to that measured by the STAR Collaboration at RHIC up to $P_T = 3$ GeV/c, independent of collision energy and centrality. The calculated results are approximately in agreement with the experimental data on the dependence of v_2 on P_T for $h^{\pm}$ in Pb-Pb collisions at $\sqrt{s_{NN}} = 2.76$ TeV. In the calculation, we take $u_1 = 0.988$ and $u_2 = 0.625 - 0.640$. The values of the expansion factor k increase with the centrality percent, and are systematically larger than those in Au-Au collisions at $\sqrt{s_{NN}} = 200$ GeV. The values σ and T also decreases with centrality percent, as that in Fig.1.

The square values of the expansion factor k^2 used for Fig.1 and Fig.2 are displayed in Figs.3, by different symbols as marked. In Au-Au and Pb-Pb collisions, $v_2(P_T)$ tends to a saturation for the more peripheral collisions(> 40%). We find that, except for the saturation region, the values of k^2 exhibit a linear dependence on centrality percent$c$. For Au-Au and Pb-Pb collisions, we have $k^2 = (3.161 \pm 0.002)c$ and $k^2 = (3.492 \pm 0.012)c$, respectively. By the geometric relation of centrality percent c to the impact parameter b, we have $c \propto b^2$, which holds to a very high accuracy for all but most peripheral collisions. Thus, the expansion factor k linearly increases with the increasing of the impact parameter b from most central (0-5%) to mid-peripheral (35-40%) collisions.

IV. CONCLUSIONS

In the above discussions, we have investigated the results of azimuthal anisotropy by using the elliptic flow v_2 vs the transverse momentum P_T for several centralities in $\sqrt{s_{NN}} = 200$ GeV Au-Au and $\sqrt{s_{NN}} = 2.76$ TeV Pb-Pb collisions. The calculated results are obtained in the framework of the multi-source idealgas model by comparing the experimental data. The calculated results are approximately in agreement with the experiment data of the STAR and ALICE Collaboration. In our model, the local sources of final observed particles are formed in heavy ion collisions. Their interaction are related to the hot dense matter in the sources, and also results in the azimuthally anisotropic expansion in the momentum space [21]. The almond shaped interaction volume produced

in a non-cental collision is converted by the pressure gradient into a momentum asymmetry. The parameter A_x in the model is used to reflect the expansion of momenta, as shown in Eq.(3). An isotropic emission corresponds to $k = 0$.

From the above comparisons, we can see that the values of the expansion factor k increases linearly with the impact parameter b increasing over the range of collision centrality (from 0-5% to 35-40%) in $\sqrt{s_{NN}}$ = 200 GeV Au-Au and $\sqrt{s_{NN}}$ = 2.76 TeV Pb-Pb collisions. It supports the idea that the increase from central to peripheral collisions reflects the expected increase due to the change in initial eccentricity of the initial fireball from central to peripheral events at each centrality [22, 23]. The difference between the two collisions is that the expansion factor of the latter one is larger than that of the former one. From RHIC to LHC energies, it is found that the average QGP specific shear viscosity η/s slightly increases [6, 24]. Recent hydrodynamic calculations in the framework of relativistic dissipative hydrodynamics have been interpreted as the evidence that the elliptic flow at RHIC energies is insensitive to the QGP viscosity and only becomes sensitive to it at LHC energies [25].

The azimuthal anisotropy resulting from the final-state particles is one of the most informative quantities in better understanding the nature and properties of the matter in high energy nuclear collisions. The ideal hydrodynamic model calculations reproduce the mass ordering of v_2 in the relatively low P_T region, but overshoot the values of v_2 for all centrality bins [26]. To understand the viscous nature of QGP, dissipative hydrodynamics has recently been applied to explain the experimental data of the collective flow parameter v_2 by including the effect of shear and bulk viscosity [27–29]. Analysis of the elliptic flow in our simple model, where the system expansion can be quantified in the momentum space, shows that the expansion factor k is characterized by the impact parameter b, which is related to participating nucleons using a realistic description of the nuclear geometry in a Glauber calculation [30] .

In summary, in the framework of the multi-source idealgas model, we have investigated the transverse momentum dependence of elliptic flow for charged particles in Au-Au collisions at the RHIC energy and in Pb-Pb collisions at the LHC energy. Our calculated results obtained in the multi-source idealgas model approximately agree with the experimental data. The expansion factor k used in the calculation exhibits a linear dependence on the impact parameter b from most central (0-5%) to mid-peripheral (35-40%) collisions. Elliptic flow has been proved to be very valuable for understanding relativistic nuclear collisions. As we know that the hydrodynamic description has gained important result over the past few years. The present work shows that the simpler multi-source idealgas model also can do the similar job. Particularly, in the descriptions of (pseudo)rapidity and multiplicity distributions for produced particles, this model is successful. In the description of the $v_2(P_T)$ at higher energies, the work is a successful attempt.

Acknowledgments. This work is supported by the National Natural Science Foundation of China under Grant No. 10975095, the National Fundamental Fund of Personnel Training Grant No. J0730317 and the Open Research Subject of the CAS Large-Scale Scientific Facility Grant No. 2060205.

[1] K. Aamodt *et al.* [The ALICE Collaboration], Phys. Rev. Lett. **105**, 252302(2010) [arXiv:1011.3914 [nucl-ex]].

[2] A. Adare *et al.* [PHENIX Collaboration], Phys. Rev. Lett. **105**, 062301 (2010) [arXiv:1003.5586 [nucl-ex]].

[3] T. Hirano, P. Huovinen and Y. Nara, arXiv:1012.3955 [nucl-th].

[4] M. Luzum, Phys. Rev. C **83**, 044911 (2011) [arXiv:1011.5173 [nucl-th]].

[5] P. Bozek, arXiv:1101.1791 [nucl-th].

[6] H. Song, S. A. Bass and U. W. Heinz, arXiv:1103.2380 [nucl-th].

[7] J. Y. Ollitrault, Phys. Rev. **D46**, 229 (1992).

[8] J. Barrette *et al.* [E877 Collaboration], Phys. Rev. Lett. **73**, 2532 (1994).

[9] J. Barrette *et al.* [E877 Collaboration], Phys. Rev. **C55**, 1420 (1997) [Erratum-ibid. **C56**, 2336 (1997)].

[10] C. Alt *et al.* [NA49 Collaboration], Phys. Rev. **C68**, 034903 (2003).

[11] K. H. Ackermann *et al.* [STAR Collaboration], Phys. Rev. Lett. **86**, 402 (2001).

[12] D. Teaney, J. Lauret and E. V. Shuryak, Phys. Rev. Lett. **86**, 4783 (2001); P. Huovinen, P. F. Kolb, U. W. Heinz, P. V. Ruuskanen and S. A. Voloshin, Phys. Lett. **B503**, 58 (2001); T. Hirano, U. W. Heinz, D. Kharzeev, R. Lacey and Y. Nara, Phys. Lett. **B636**, 299 (2006);
P. Romatschke and U. Romatschke, Phys. Rev. Lett. **99**, 172301 (2007).

[13] H. Song and U. W. Heinz, Phys. Lett. **B658**, 279 (2008);
H. Song and U. W. Heinz, Phys. Rev. **C77**, 064901 (2008).

[14] F. H. Liu, J. S. Li and M. Y. Duan, Phys. Rev. **C75**, 054613 (2007).

[15] J. X. Sun, F. H. Liu, E. Q. Wang, Y. Sun and Z. Sun, Phys. Rev. C **83**, 014001 (2011).

[16] F. H. Liu, N. N. Abd Allah and B. K. Singh, Phys. Rev. C **69**, 057601 (2004).

[17] H. Sorge, Phys. Rev. Lett. **78**, 2309 (1997) [arXiv:nucl-th/9610026].

[18] H. J. Drescher, A. Dumitru, C. Gombeaud and J. Y. Ollitrault, Phys. Rev. C **76**, 024905 (2007) [arXiv:0704.3553 [nucl-th]].

[19] R. Snellings, arXiv:1102.3010 [nucl-ex].

[20] P. Huovinen and P. V. Ruuskanen, Ann. Rev. Nucl. Part. Sci. **56**, 163 (2006).

[21] T. Song, C. M. Ko, S. H. Lee and J. Xu, arXiv:1008.2730 [hep-ph].

[22] R. S. Bhalerao, J. P. Blaizot, N. Borghini and J. Y. Ollitrault, Phys. Lett. B **627**, 49 (2005) [arXiv:nucl-th/0508009].

[23] W. Broniowski, P. Bozek and M. Rybczynski, Phys. Rev. C **76**, 054905 (2007) [arXiv:0706.4266 [nucl-th]].

[24] V. Roy and A. K. Chaudhuri, arXiv:1103.2870 [nucl-th].

[25] H. Niemi, G. S. Denicol, P. Huovinen, E. Molnar and D. H. Rischke, arXiv:1101.2442 [nucl-th].

[26] B. I. Abelev *et al.* [The STAR Collaboration], Phys. Rev. **C81**, 044902 (2010).

[27] G. S. Denicol, T. Kodama and T. Koide, arXiv:1002.2394 [nucl-th].

[28] C. Shen and U. Heinz, arXiv:1101.3703 [nucl-th].

[29] B. Schenke, S. Jeon and C. Gale, arXiv:1102.0575 [hep-ph].

[30] M. L. Miller, K. Reygers, S. J. Sanders and P. Steinberg, Ann. Rev. Nucl. Part. Sci. **57**, 205 (2007) [arXiv:nucl-ex/0701025].

TABLE I: Values of parameters k and σ in our calculations.

Figure	Centrality	σ(GeV/c)	k(GeV/c)	χ^2/dof
Fig.1	50%-60%	1.119 ± 0.006	1.076 ± 0.001	0.707
	45%-50%	1.127 ± 0.004	1.069 ± 0.002	0.716
	40%-45%	1.141 ± 0.011	1.059 ± 0.005	0.643
	35%-40%	1.164 ± 0.016	1.046 ± 0.008	0.622
	30%-35%	1.204 ± 0.024	0.991 ± 0.010	0.495
	25%-30%	1.262 ± 0.025	0.936 ± 0.012	0.413
	20%-25%	1.336 ± 0.028	0.875 ± 0.024	0.244
	15%-20%	1.365 ± 0.020	0.719 ± 0.052	0.192
	10%-15%	1.402 ± 0.019	0.586 ± 0.045	0.165
	5%-10%	1.452 ± 0.016	0.426 ± 0.042	0.146
	0%- 5%	1.551 ± 0.016	0.264 ± 0.036	0.104
Fig.2	40%-50%	1.192 ± 0.020	1.116 ± 0.002	0.808
	30%-40%	1.248 ± 0.022	1.110 ± 0.004	0.244
	20%-30%	1.344 ± 0.018	0.942 ± 0.056	0.124
	10%-20%	1.486 ± 0.015	0.725 ± 0.044	0.116

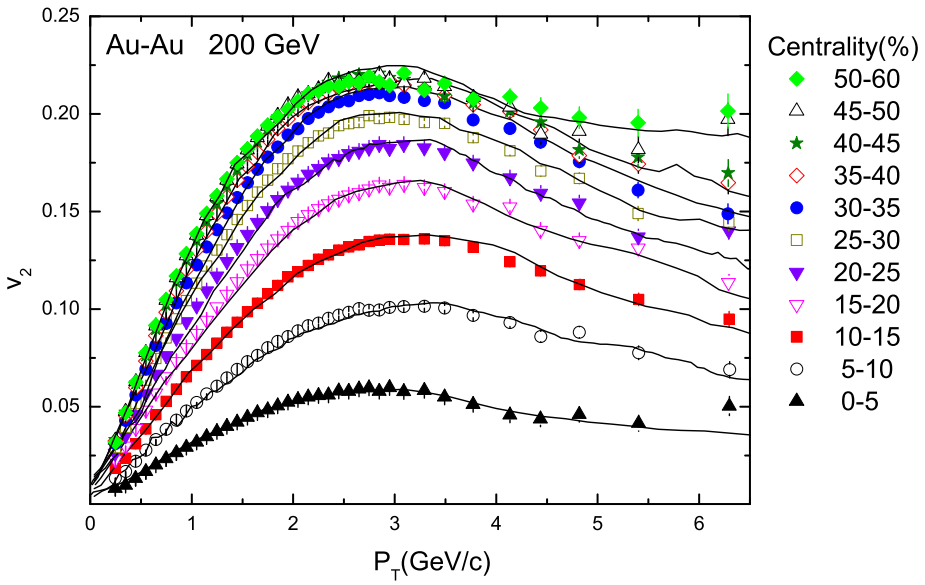


FIG. 1: P_T dependence of v_2 for charge hadrons in Au-Au collisions at $\sqrt{s_{NN}}$ = 200 GeV. Experimental data taken from the STAR Collaboration [2] are shown with the scattered symbols. Our results calculated from the multi-source idealgas model are shown with the curves.

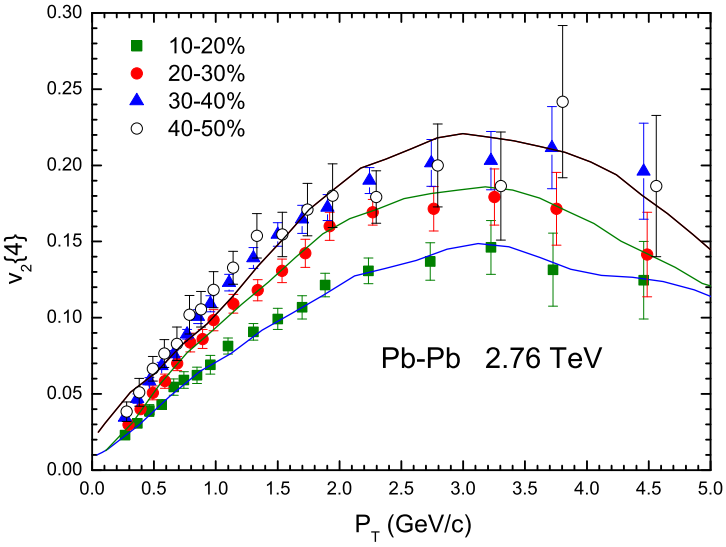


FIG. 2: P_T dependence of v_2 for charge hadrons in Pb-Pb collisions at $\sqrt{s_{NN}}$ = 2.76 TeV. Experimental data taken from the ALICE Collaboration [1] are shown with the scattered symbols. Our results calculated from the multi-source model idealgas are shown with the curves.

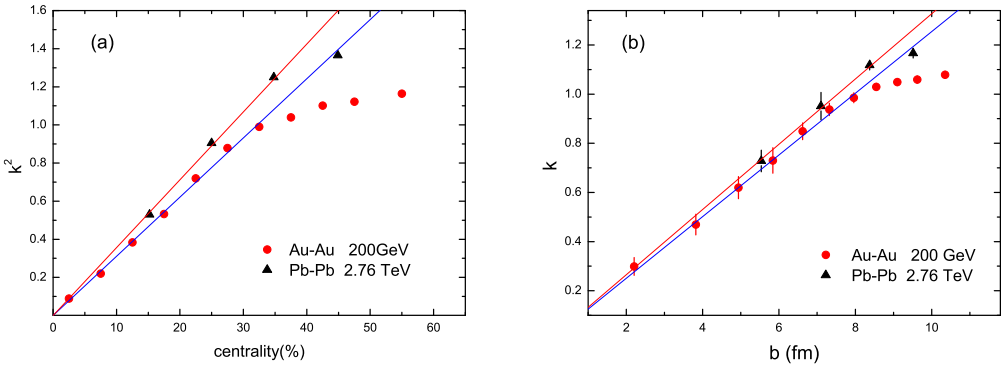


FIG. 3: Centrality and the impact parameter *b* dependence of the square of the expansion factor k^2. The symbols represent the parameter values used in Figs.1-2. The lines are a fitted results.